



**HAL**  
open science

## Measurement and modelling of gaseous elemental iodine (I<sub>2</sub>) dry deposition velocity on grass in the environment

Oumar Telly Bah, Didier Hebert, Olivier Connan, Luc Solier, Philippe Laguionie, D.L. Bourles, Denis Maro

### ► To cite this version:

Oumar Telly Bah, Didier Hebert, Olivier Connan, Luc Solier, Philippe Laguionie, et al.. Measurement and modelling of gaseous elemental iodine (I<sub>2</sub>) dry deposition velocity on grass in the environment. *Journal of Environmental Radioactivity*, 2020, 219, pp.106253. 10.1016/j.jenvrad.2020.106253 . hal-03146199

**HAL Id: hal-03146199**

**<https://hal.science/hal-03146199>**

Submitted on 18 Feb 2021

**HAL** is a multi-disciplinary open access archive for the deposit and dissemination of scientific research documents, whether they are published or not. The documents may come from teaching and research institutions in France or abroad, or from public or private research centers.

L'archive ouverte pluridisciplinaire **HAL**, est destinée au dépôt et à la diffusion de documents scientifiques de niveau recherche, publiés ou non, émanant des établissements d'enseignement et de recherche français ou étrangers, des laboratoires publics ou privés.



Distributed under a Creative Commons Attribution - NonCommercial - NoDerivatives 4.0 International License

# 1 Measurement and modelling of gaseous elemental iodine (I<sub>2</sub>) dry 2 deposition velocity on grass in the environment

3

4 Oumar Telly Bah<sup>(1,2)\*</sup>, Didier Hébert<sup>1</sup>, Olivier Connan<sup>1</sup>, Luc Solier<sup>1</sup>, Philippe Laguionie<sup>1</sup>, Didier Bourlès<sup>2</sup>, Denis Maro<sup>1</sup>.

5 <sup>1</sup>Institut de Radioprotection et de Sûreté Nucléaire, PSE-ENV/SRTE/LRC, BP 10, Rue Max-Pol Fouchet, 50130 Cherbourg  
6 Octeville, France.

7 oumar-telly.bah@irsn.fr, didier.hebert@irsn.fr, olivier.connan@irsn.fr, luc.solier@irsn.fr, philippe.laguionie@irsn.fr  
8 denis.maro@irsn.fr

9 <sup>2</sup>Aix-Marseille Univ., CNRS, IRD, INRAE, Coll France, UM 34 CEREGE, Technopôle de l'Environnement Arbois-  
10 Méditerranée, BP80, 13545 Aix-en-Provence, France.

11 bourles@cerege.fr

12 \* Corresponding author:

13 [E-mail address: oumar-telly.bah@irsn.fr](mailto:oumar-telly.bah@irsn.fr)

14 *IRSN*

15 *Cherbourg-Octeville Radioecology Laboratory (LRC)*

16 *Rue Max Pol Fouchet*

17 *BP10- 50130 Cherbourg-Octeville*

18 *Tel: +33 (0)2 33 01 41 16*

19

## 20 Abstract

21 Assessing the impact of radioactive iodine on humans subsequent to a nuclear accident requires a better understanding of its  
22 behaviour in the environment. An original approach aimed at developing a model constrained by data collected during  
23 experimental campaigns has been developed. These experimental campaigns, named MIOSEC 2 and MIOSEC 3  
24 respectively, were conducted in the middle of grassland. They are based on emissions of gaseous elemental iodine (I<sub>2</sub>) into  
25 the atmosphere above the grassland to determine the dry deposition velocities of iodine on the grass and to model these  
26 velocities as a function of the environmental conditions, particularly wind friction velocity, sensible heat flux, and stomatal  
27 resistance. The measured dry deposition velocities were between 0.02 and 0.49 cm.s<sup>-1</sup> during MIOSEC 2, varying by more  
28 than one order of magnitude, and between 0.48 and 1.25 cm.s<sup>-1</sup> during MIOSEC 3. The dry deposition model for iodine  
29 developed as a result of these experiments relies on the micrometeorological characteristics of the atmospheric surface  
30 layer, the pertinent physical and chemical properties of the iodine and the surface properties of the grass; all these  
31 parameters were measured at the time of the experiments. Given the experimental conditions, the modelled dry deposition  
32 velocities varied between 0.11 and 0.51 cm.s<sup>-1</sup> during MIOSEC 2 and between 0.31 and 1.6 cm.s<sup>-1</sup> during MIOSEC 3. The  
33 dry deposition model for iodine indicates that the variations in deposition velocity are induced by the mechanical  
34 turbulence, since there is significant correlation between the dry deposition velocities of iodine and the wind friction  
35 velocities on grass. The model also shows that the higher deposition velocity values during MIOSEC 3 are due to the fact

36 that the stomata were more open during the experiments. There is also significant correlation between the experimental  
37 results and modelled values both for MIOSEC 2 ( $R^2 = 0.61$ ) and for MIOSEC 3 ( $R^2 = 0.71$ ).

38  
39 *Keywords:* Elemental iodine, environment, emission, grass, dry deposition velocity.

---

## 40 1. Introduction

41 Iodine is a trace element in the halogen family. It is essential for thyroid function in animals. Iodine has 37 isotopes  
42 with mass numbers ranging from 108 to 144. Iodine-127 is the only stable isotope of iodine. All the other isotopes of iodine  
43 are radioactive. Thirteen are fission products, including iodine-129 which has the longest half-life (15.7 million years) and  
44 iodine-131 which has a half-life of 8.02 days. Most iodine is found in the marine environment (>70%), in dissolved forms at  
45 concentrations of between 45 and 60  $\mu\text{g.L}^{-1}$  (Fuge, 1996; Wong, 1991). It can also be found on land at concentrations  
46 influenced, among other parameters, by proximity to oceans, by the organic composition of the environment, by ground  
47 topography and by the bioavailability of molecules containing iodine. The mechanisms of iodine transfer into the  
48 atmosphere from marine and terrestrial environments are not known, but the most likely is volatilization. In acid condition,  
49 the iodine present in seawater in ionic form is liable to volatilize as  $\text{I}_2$ , whereas in neutral or alkaline condition,  
50 volatilization is unlikely (Fuge, 1996; Hou et al., 2009). In addition, iodine can volatilize in the form of organic compounds,  
51 e.g.  $\text{ICH}_3$ , due to the oxidation of residues of plants such as seaweed (Fuge, 1996; Whitehead, 1984). The iodine ( $^{127}\text{I}$ )  
52 concentrations measured in the atmosphere are between 10 and 100  $\text{ng.m}^{-3}$ , taking account of all physico-chemical forms  
53 (Truesdale et al., 2012). Other sources of atmospheric iodine ( $^{129}\text{I}$  and/or  $^{131}\text{I}$ ) are spontaneous uranium ( $^{238}\text{U}$ ) fission,  
54 nuclear testing, releases from spent fuel reprocessing plants and emissions from nuclear power plants in normal or accident  
55 operating conditions.

56 During a nuclear accident, radioactive iodine ( $^{131}\text{I}$ ) is released into the environment (Parache et al., 2011; Zhou,  
57 1995). In the atmosphere, radioactive iodine diffuses in the same way as any other gas (Chamberlain and Chadwick, 1966).  
58 With oxidation states ranging from -1 to +5, the overall biogeochemical cycle of iodine is quite complex and involves  
59 various processes (Carpenter, 2003; Saiz-Lopez et al., 2012). Its high reactivity means that iodine, including radioactive  
60 iodine, changes rapidly in the environment through photolysis and reacts with other atmospheric compounds including  
61 ozone and nitrogen compounds (Carpenter, 2003; Hou et al., 2009; Noguchi and Murata, 1988). Because of this, radioactive  
62 iodine is present in the atmosphere in several physico-chemical forms: particulate (associated with atmospheric aerosol  
63 particles) and gaseous. The gaseous forms are inorganic:  $\text{I}_2$ , HI, HIO, and organic:  $\text{CHI}_3$ ,  $\text{CH}_2\text{I}_2$ ,  $\text{CH}_3\text{CH}_2\text{CH}_2\text{I}$ . Radioactive  
64 iodine concentrations can vary not only according to distance from the discharge stack (Thakur et al., 2013), but also  
65 according to season and climate when the radioactive half-life allows (Hou et al., 2009).

66 Subsequent to an accident, particular attention should be paid to the deposition mechanism of the iodine, which can  
67 be found in cows' milk via grazing, then in humans by milk drinking or by direct ingestion of fresh vegetables, where it can  
68 cause thyroid cancer. Deposition can occur in dry weather (dry deposition) or wet weather (wet deposition), and is  
69 quantified by velocity. Numerous studies have shown that the dry deposition velocities of iodine are highly dependent on  
70 the one hand on the state of iodine in the atmosphere: gaseous or particulate including in this last case the particle size, and  
71 on the other on the chemical species encountered (Nielsen, 1981; Noguchi and Murata, 1988). On grass, the dry deposition

72 velocity of gaseous elemental iodine measured in the environment by Chamberlain and Chadwick (1966) was  $1.8 \text{ cm.s}^{-1}$ ,  
73 while Karunakara et al. (2018) measured dry deposition velocities of between  $0.5 \times 10^{-3}$  and  $3.3 \times 10^{-3} \text{ cm.s}^{-1}$  in an  
74 environmental chamber. These values differ by several orders of magnitude, since no parameterisation was done for  
75 meteorological values or surface properties of the grass.

76 This study aims to quantify and model the dry deposition velocities of gaseous elemental iodine ( $\text{I}_2$ ) on grass based  
77 on experiments conducted in the environment. The experiments consisted in emitting gaseous elemental iodine into the  
78 atmosphere during a limited period of time in the absence of precipitation and quantifying the quantities of iodine deposited  
79 on grass test specimens placed downwind of the emission point. In case of rain during  $\text{I}_2$  emission,  $\text{I}_2$  can be absorbed by the  
80 rain drops, which will lead to modification of global transfer depending on the solubility of iodine and rain intensity (via  
81 drops size) and consequently, a modification of the deposition velocity. Because the average iodine concentrations in the  
82 atmosphere above the test specimens were known, dry deposition velocities were calculated and parameterised for wind  
83 friction velocity, sensible heat flux and stomatal resistance.

## 84 2. Methodology

### 85 *A. Measurement of iodine dry deposition velocities on grass*

#### 86 *1. Equations*

87 The iodine dry deposition velocities were calculated by dividing the iodine dry deposition fluxes by the atmospheric  
88 concentrations of iodine. For this purpose, the iodine dry deposition fluxes were obtained by dividing the iodine  
89 concentrations measured on the grass by the iodine emission time (Eq. (1)). The deposition velocities were then determined  
90 by dividing the mean iodine dry deposition fluxes on the 2 squares of grass for each of the experiments by the mean  
91 atmospheric iodine concentrations in the corresponding 2 bubbler flasks (Eq. (2)).

$$F = -C_d/t \quad (1)$$

92 Where  $F$  is the iodine dry deposition flux ( $\mu\text{g.m}^{-2}.\text{s}^{-1}$ );  $C_d$  is the iodine concentration deposited on the grass ( $\mu\text{g.m}^{-2}$ ) and  $t$  is  
93 the emission time (s).

$$V_d = -F/C_a(z) \quad (2)$$

94 Where  $V_d$  is the iodine dry deposition velocity ( $\text{m.s}^{-1}$ ) and  $C_a(z)$  the atmospheric iodine concentration ( $\mu\text{g.m}^{-3}$ ) at the height  
95  $z$  at which the air is sampled.

96 To obtain the iodine concentrations in the air and on the grass, several experiments based on gaseous elemental  
97 iodine emissions were conducted on an experimental site in the middle of grassland.

#### 98 *2. Description of the measurement site*

99 Two experimental campaigns, entitled MIOSEC 2 and MIOSEC 3, were conducted in the middle of grassland on an  
100 experimental site of the French National Institute for Agricultural Research (INRA) at Lusignan (France) ( $46^\circ 24', 02''\text{N}$ ;  $0^\circ 7'$ ,

101 04'E). MIOSEC 2 ran from 18 to 26 September 2018 and MIOSEC 3 from 4 to 7 June 2019. During MIOSEC 2, at any  
 102 point approximately 500 m from the experiment, the grass was 0.10 m high and its mean roughness length ( $z_0$ ) was 0.01 m.  
 103 During MIOSEC 3, at any point approximately 500 m from the experiment, the grass was 0.15 m high and its mean  
 104 roughness length ( $z_0$ ) was 0.015 m (Table 1). The roughness lengths given are approximated on the basis of the grass height  
 105 ( $z_0/z = 0.1$ ) (Pellerin et al., 2017). During the two measurement campaigns, the grass consisted mainly of *Lolium perenne*  
 106 and *Dactylis*.

107

108 **Table 1:** Description of the measurement site.

Campaign (Date)	Type of cover (height)	Roughness length ( $z_0$ )	Surface homogeneity
MIOSEC 2 (18 to 26 September 2018)	Grassland (0.10 m)	0.01 m	> 500 m
MIOSEC 3 (4 to 7 June 2019)	Grassland (0.15 m)	0.015 m	> 500 m

109  
110

### 111 3. Iodine emissions

112 The measurement campaigns use gaseous elemental iodine emissions produced using an iodine generator designed  
 113 previously. To generate the iodine, 20 ml of a KI solution (25 g.L<sup>-1</sup>) are added drop by drop to a mixture of 100 ml of H<sub>2</sub>SO<sub>4</sub>  
 114 (10%) and 100 ml of H<sub>2</sub>O<sub>2</sub> (35%) for 30 minutes. Each iodide (I<sup>-</sup>) droplet added to the mixture leads to the formation in  
 115 solution of gaseous elemental iodine (I<sub>2</sub>). The gaseous form I<sub>2</sub> is entrained by a 2 L.min<sup>-1</sup> air flow running continuously for  
 116 the 30-minute emission duration. A filter is placed at the iodine generator output to stop any iodine particles that might form  
 117 inside the tube connected to the generator output (Fig. 1).

118 The homogeneity of iodine release from generator was validated during the generator design. Two flask each  
 119 containing 100 ml of NaOH (0.5 N) are directly connected to the output of generator to trap iodine. In the event that the  
 120 totality of iodine is not trapped in the first flask, the iodine excess is trapped in the second. Each 5 minutes, iodine  
 121 generation is stopped, and the 2 flasks are replaced by 2 others. This operation is repeated 6 times, corresponding to the total  
 122 duration of iodine emission (30 minutes). The measurement of the total iodine in the first flask validated the protocol for  
 123 iodine trapping in 100 ml of NaOH (0.5 N). Iodine concentrations measured in the different flasks are the same.  
 124 Consequently, iodine release from generator is homogeneous during the 30 minutes.

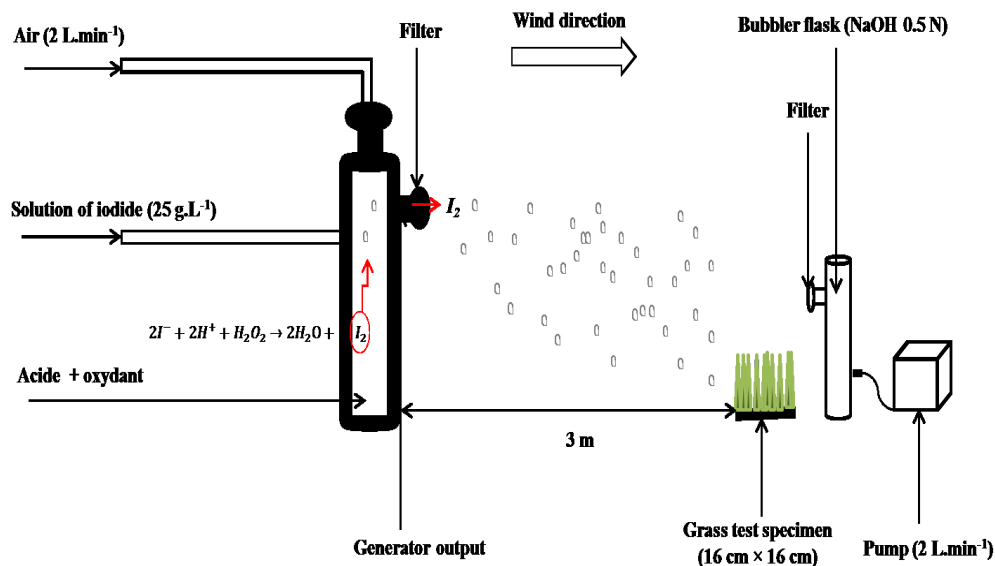


Fig. 1. Emission of gaseous elemental iodine, sampling from the atmosphere and grass.

#### 4. Collection and treatment of the samples (including blanks)

Two cellulose filters (0.45  $\mu\text{m}$ ) are placed between the emission point and the sampling points to collect any iodine particles that form during emission. Depending on the wind direction, 2 squares of grass (*Lolium perenne*) measuring 16 cm  $\times$  16 cm each are placed 3 m from the generator output to collect the deposited iodine. Each experiment being carried out during 30 minutes and “field loss half-life” for elemental iodine being determined (13 days) on grassland in the growing season (Whitehead, 1984), re-volatilization is therefore very low during 30 minutes and has not been determined.

Two flasks, each containing 100 mL of NaOH (0.5 N) are placed approximately 5 cm from the squares of grass to collect the atmospheric iodine, by means of sparging at a rate of 2 L.min<sup>-1</sup> using a pump connected to the flask output (Fig. 1). A filter is placed at the input of each bubbler flask to collect any iodine particles. 14 and 8 experiments were conducted during MIOSEC 2 and MIOSEC 3, respectively. After each experiment, the sample were collected and treated.

For each of the experiments, a grass blank and an atmospheric blank were made by placing at 50 m from emission point, a 16 cm  $\times$  16 cm square of grass and a bubbler flask containing 100 ml of NaOH (0.5 N), respectively.

The particulate iodine fraction was collected by placing each of the filters in 50 ml of NaOH (0.5 N). After vigorous homogenisation, the whole mixture was filtered.

To determine the quantities of iodine emitted into the atmosphere, the samples collected from the bubbler flasks were filtered. The atmospheric blank was treated in the same way as the samples from the bubbler flasks.

The quantities of iodine deposited were determined from the grass. The squares of grass were cut so as to collect the maximum mass. To extract iodine from grass samples, an original methodology was developed. Iodine was separated from grass using calcination at 400  $^{\circ}\text{C}$  (Table 2) followed by liquid-liquid extraction (Fig. 2). Firstly, each square of cut grass was placed in a flask containing 150ml of NaOH (5 N). A physico-chemical treatment was then applied to the samples. The

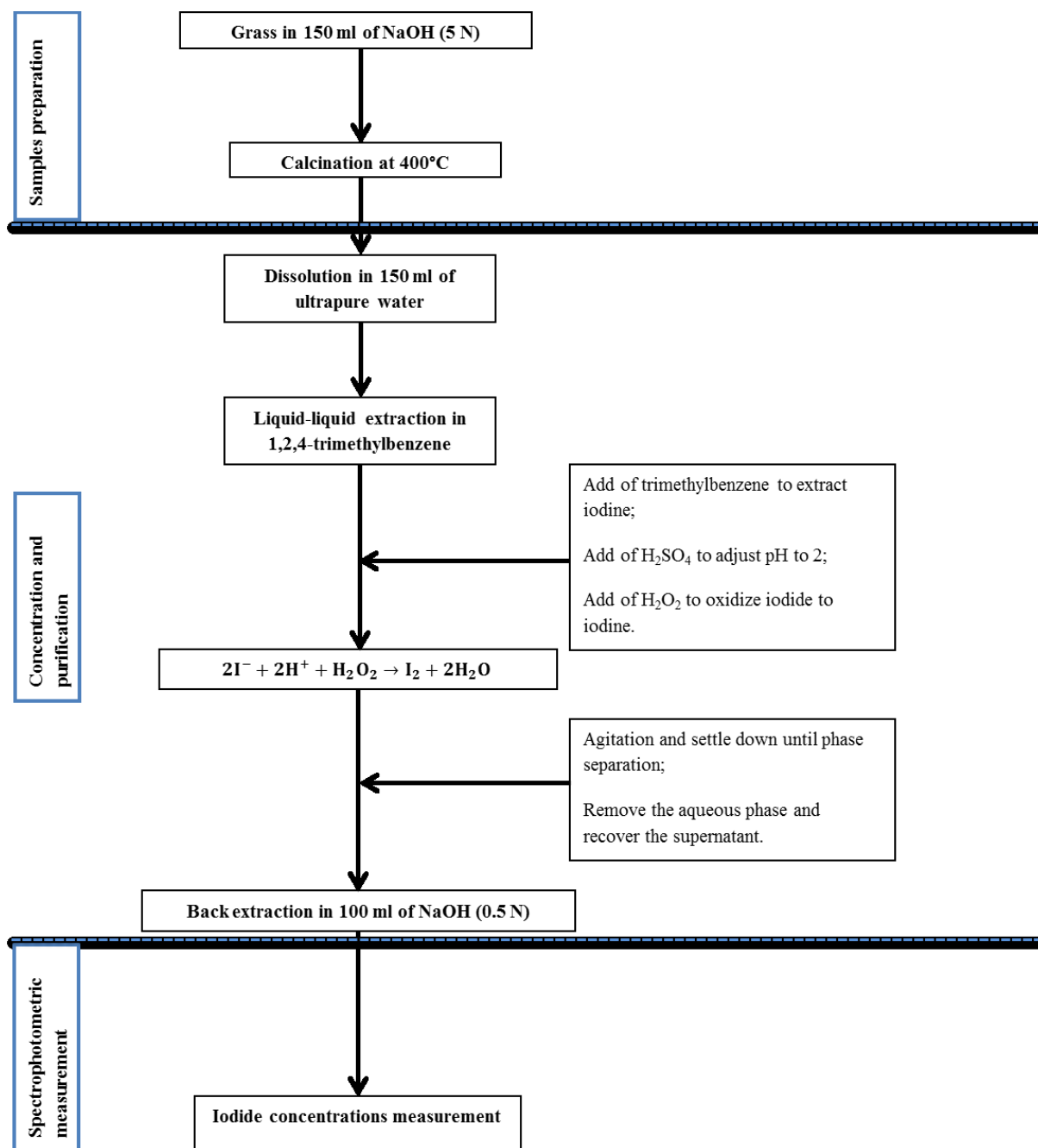
149 samples were placed in porcelain crucibles and calcined at 400°C to destroy organic matter. After cooling, each sample was  
 150 dissolved in 150 ml of ultrapure water (18.2 MΩ cm at 25°C) and then filtered. Iodine is recovered from the filtrate as  
 151 iodide form. H<sub>2</sub>SO<sub>4</sub> (30%) was added to adjust pH to 2 and H<sub>2</sub>O<sub>2</sub> (35%) to oxidize iodide to iodine. After agitation and  
 152 settle down until phase separation, iodine in solution is released and trapped by trimethylbenzene as I<sub>2</sub> form. The aqueous  
 153 phase was eliminated and the phase containing the trimethylbenzene was isolated and washed with ultrapure water until its  
 154 pH was neutral. Then 100 ml of NaOH (0.5 N) was added to extract the iodine in the form I<sup>-</sup> (back extraction). The grass  
 155 blank was treated in the same way as the grass samples (Fig. 2).

156

157 **Table 2:** Calcination cycle to separate the iodine (<sup>127</sup>I) from the grass.

Step	Temperature (°C)	Duration (min)
1	25-100	75
2	100-100	120
3	100-200	100
4	200-200	120
5	200-400	200
6	400-400	120
7	400-25	375

158 To determine the extraction efficiency, grass blank and 12 tests were performed. For each test, 5 ml of KI (1g.L<sup>-1</sup>)  
 159 were added to 20 g of fresh grass. After adding 150 ml of NaOH (5 N), the whole mixture was treated in accordance with  
 160 the sample preparation protocol (Fig. 2). The blank was processed in the same way as the tests, replacing the KI with  
 161 ultrapure water.



162  
163 Fig. 2. Processing of grass samples for spectrophotometric measurement.  
164

165 *5. Iodine measurement by colorimetry*

166 All the samples were measured by UV-visible spectrophotometry (Safas, UVmc1). The colorimetry technique for  
167 iodine measurement is based on the Sandell and Kolthoff (1937) method; the reaction between the cerium ions and the  
168 arsenic ions is catalysed by the iodide ions. The absorption measured by spectrophotometry at 415 nm is then inversely

169 proportional to the iodide concentration. The detection limit is  $2.5 \mu\text{g.L}^{-1}$ . The iodine concentrations measured in the  
170 atmosphere are expressed in  $\mu\text{g.m}^{-3}$  and those measured on the grass in  $\mu\text{g.m}^{-2}$ .

## 171 *B. Environmental (including meteorological) variable measurements*

172 An ultrasonic anemometer (Young 81000V, Inc.) set to a frequency of 10 Hz and installed 50 cm above the ground,  
173 and a weather station (Spectrum, Watchdog 2700, Inc.) were used to acquire the meteorological data. The direction ( $^{\circ}$ ),  
174 velocity (u) and friction velocity ( $u^*$ ) of the wind, sensible heat flux (H), Monin-Obukhov length (L) and atmospheric  
175 stability ( $1/L$ ) were measured by the ultrasonic anemometer, and the temperature ( $T_s$ ), relative humidity (RH), total solar  
176 radiation (SR) and photosynthetically active radiation (PAR) were measured by the weather station.

## 177 *C. Modelling of the dry deposition velocities of iodine*

### 178 *1. Model description and identification of the input variables*

179 The dry deposition velocity of a gas refers to the transfer of that gas from the air to surfaces (soil, water, vegetation)  
180 (Arya, 1999) in the absence of precipitation. It is complex and varies significantly according to:

- 181     ▪ the micrometeorological characteristics of the atmospheric surface layer because of the turbulent transport that can  
182         occur in that layer;
- 183     ▪ the physical and chemical properties of the diffusing species;
- 184     ▪ the physical and chemical properties of the surface cover.

185 The dry deposition velocity of a gas has been defined as the inverse of the sum of the three types of resistance to the  
186 dry deposition of that gas, namely the aerodynamic resistance, the laminar sublayer resistance and the canopy resistance or  
187 surface resistance. The expression used to determine  $V_d$  (Eq. (3)) was given by Seinfeld (1985).

$$V_d = \frac{1}{R_a + R_b + R_c} \quad (3)$$

188 Where  $V_d$  is the dry deposition velocity ( $\text{m.s}^{-1}$ );  $R_a$  is the aerodynamic resistance ( $\text{s.m}^{-1}$ );  $R_b$  is the laminar sublayer  
189 resistance ( $\text{s.m}^{-1}$ ) and  $R_c$  is the canopy resistance or surface resistance ( $\text{s.m}^{-1}$ ).

190 The input parameters (Table 3) used to model the deposition velocities were the parameters related to the physico-chemical  
191 properties of the iodine, the surface properties of the grass and the sampling conditions, i.e.:

- 192     ▪ Reference values: diameter of an iodine molecule ( $D_p$ ), canopy aerodynamic resistance ( $R_{ac0}$ ), ground resistance  
193         ( $R_{g0}$ ), cuticle resistance ( $R_{cut0}$ ) and mesophyll resistance ( $R_m$ );
- 194     ▪ Variables: leaf area index (LAI), roughness length of the grass ( $z_0$ ), measurement height ( $z$ ) and minimum stomatal  
195         resistance ( $r_i$ ).

196  
197  
198

199 Table 3: Input parameters of the model for dry deposition of iodine.

Campaign (Date)	$D_p$ (m)	$z$ (m)	$z_0$ (m)	LAI	$ri$ ( $s.m^{-1}$ )	$R_m$ ( $s.m^{-1}$ )	$R_{ac0}$ ( $s.m^{-1}$ )	$R_{g0}$ ( $s.m^{-1}$ )	$R_{cut0}$ ( $s.m^{-1}$ )
MIOSEC 2 (18 to 26 September 2018)	$2.8 \times 10^{-8}$	0.26	0.01	1.5	9999	0	1000	100	50
MIOSEC 3 (4 to 7 June 2019)	$2.8 \times 10^{-8}$	0.26	0.01	1.5	60	0	1000	100	50

200

## 201 2. Determination of the resistances ( $R_a$ , $R_b$ and $R_c$ ) and the input variables of the model

202 Aerodynamic resistance refers to the aerodynamic component of transfer governed by microturbulence. It therefore  
 203 corresponds to the resistance to vertical transfer to the surfaces in the immediate vicinity of the elements (gas, aerosols)  
 204 through the atmospheric surface layer. The lower limit of the atmospheric surface layer is the roughness length. Of the  
 205 micrometeorological parameters that influence aerodynamic resistance, wind friction velocity and atmospheric stability are  
 206 the most important (Arya, 1999). The expressions for  $R_a$  and  $R_b$  shown respectively in Eqs. (4) and (5) have been defined by  
 207 Padro et al. (1991).

$$R_a = \frac{1}{k u^*} \left[ 0.74 \ln \left( \frac{z}{z_0} \right) - \Psi_H \right]$$

With,

$$\Psi_H = \begin{cases} -4.7 \frac{z}{L} & 0 < \frac{z}{L} < 1 \text{ (stable condition )} \\ 2 \cdot 0.74 \ln \left[ \frac{(1+y)}{2} \right], & y = \left( 1 - 9 \frac{z}{L} \right)^{\frac{1}{2}} & -1 < \frac{z}{L} < 0 \text{ (unstable condition )} \end{cases} \quad (4)$$

208 Where  $u^*$  is the wind friction velocity ( $ms^{-1}$ );  $k$  is the Von Karman constant ( $k=0.4$ );  $z$  is the reference height at which the  
 209 deposition velocity is evaluated, i.e. the height from the ground at which the air is sampled;  $z_0$  is the roughness length;  $\Psi_H$  is  
 210 the stability correction function for heat and  $L$  is the Monin-Obukhov length.

211 During the 2 measurement campaigns, the roughness length of the grass and the air sampling height were 0.01 m and  
 212 0.26 m respectively. Depending of Pasquill stability classes, the experiments were carried out under stable, unstable and  
 213 neutral atmospheric conditions (see Table 7 and Table 8). Equation (4) was applied according to the stable case and unstable  
 214 case defined by author. In neutral condition,  $\Psi_H = 1$  (Seinfeld and Pandis, 2016) was used for  $R_a$  calculation.

215 Laminar sublayer resistance ( $R_b$ ) is the resistance to diffusion of the elements through the molecular sublayer in direct  
 216 contact with the surface.  $R_b$  depends on both turbulence and molecular diffusion (Eq. (5)).

$$R_b = \frac{z}{k u^*} \left( \frac{v}{D_i} \right)^{\frac{2}{3}} \quad (5)$$

217 Where  $\nu$  is the kinematic viscosity of the air ( $\nu = 1.5 \times 10^{-5} \text{ m}^2.\text{s}^{-1}$ ) and  $D_i$  is the molecular diffusivity (Eq. (6)) of a species  $i$   
 218 in the air (Seinfeld, 1985).

219 With,

$$D_i = \frac{k_B T C_u}{6\pi \mu D_p} \quad (6)$$

220 Where  $K_B$  is the Boltzmann constant ( $K_B = 1.38 \times 10^{-23} \text{ K.J}^{-1}$ );  $T$  is the temperature (K);  $C_u$  is the Cunningham correction  
 221 factor for small particles or molecules with a diameter of less than  $1 \mu\text{m}$ ;  $\mu$  is the dynamic viscosity coefficient of air ( $1.8 \times$   
 222  $10^{-5} \text{ kg.m}^{-1}.\text{s}^{-1}$ );  $D_p$  is the diameter of the gas molecule studied. The diameter of a gaseous iodine molecule ( $I_2$ ) is  $2.8 \times 10^{-10}$   
 223 m (Forsythe, 1956). The Cunningham correction (Eq. (7)) was given by Seinfeld (1985).  $\lambda$  is the mean free path of a  
 224 molecule. At ambient pressure and temperature:  $\lambda = 6.8 \times 10^{-8} \text{ m}$ .

$$C_u = 1 + \frac{\lambda}{D_p} \left( 2.54 + 0.8 \exp \left( -\frac{0.55 D_p}{\lambda} \right) \right) \quad (7)$$

225 The overall resistance on the surface of the cover ( $R_c$ ), called the "surface resistance" or "canopy resistance",  
 226 includes the stomatal resistance and the non-stomatal resistance. For surfaces with plant cover, the model used most  
 227 frequently to describe  $R_c$  is the model defined by Zhang et al. (2002b).  $R_c$  was determined using Eq. (8) as defined in Zhang  
 228 et al. (2002a).

$$\frac{1}{R_c} = \frac{1 - W_{st}}{R_{st} + R_m} + \frac{1}{R_{ns}} \quad (8)$$

229 Where  $R_c$  is the surface resistance ( $\text{s.m}^{-1}$ );  $R_{st}$  ( $\text{s.m}^{-1}$ ) is the stomatal resistance;  $R_m$  ( $\text{s.m}^{-1}$ ) is the mesophyll resistance;  $R_{ns}$   
 230 ( $\text{s.m}^{-1}$ ) is the non-stomatal resistance and  $W_{st}$  is the stomatal blocking fraction (no unit).

231 The stomatal resistance is the resistance to opening of the stomata. In other words, it is the resistance to gas  
 232 absorption by the blades of grass. It is the result of biological processes on the surface of the plant cover. Consequently, the  
 233 properties of the grass are very important to the final stage of the deposition process. The parameters influencing stomatal  
 234 resistance are (Arya, 1999):

- 235 - the properties of the plant cover, including the water potential, roughness and leaf area index (LAI). The LAI is the  
 236 area developed by the blades of grass per unit of ground surface area. It is a value that has no physical dimension.  
 237 It was determined using an LAI-meter (LICOR, LAI-2000);
- 238 - the physico-chemical properties of the gas, including solubility and molecular diffusivity;
- 239 - the weather conditions, particularly the vapour-pressure deficit, temperature and solar radiation.

240 The stomatal resistance was calculated using an empirical formula (Eq. (9)) developed by (Wesely, 1989).

$$R_{st} = r_i \{ 1 + [200(SR + 0,1)^{-1}]^2 \} \{ 400[T_s(40 - T_s)]^{-1} \} \quad (9)$$

241 Where  $SR$  is the total solar radiation in ( $\text{W.m}^{-2}$ );  $T_s$  is the air temperature ( $^{\circ}\text{C}$ ) between  $0$  and  $40^{\circ}\text{C}$  and  $r_i$  ( $\text{s.m}^{-1}$ ) is the  
 242 minimum stomatal resistance for water vapour. The last of these varies according to the type of plant cover, the season but

243 also the chemical species. The meteorological data used for the parameterisation of  $R_{st}$  were obtained using the weather  
 244 station and correspond to the experiment periods (Table 7 and Table 8). Depending of seasons and landuse type, as urban  
 245 land, deciduous forest or grassland, Wesely (1989) have defined the values of  $r_i$ . The values of  $r_i$  corresponding to grassland  
 246 are given in Table 4. Given that MIOSEC 2 and MIOSEC 3 ran from 18 to 26 September 2018 and from 4 to 7 June 2019,  
 247 the values  $r_i = 9999$  ( $s.m^{-1}$ ) and  $r_i = 60$  ( $s.m^{-1}$ ) respectively were selected for the calculation of  $R_{st}$ .

248

249 **Table 4:**  $r_i$  ( $s.m^{-1}$ ) values for grassland according to season (Wesely, 1989).

Period of the year	$r_i$ ( $s.m^{-1}$ )
Summer	60
Autumn before harvest	9999
Late autumn with frost but no snow	9999
Winter with snow	9999
Spring	120

250

251 Equation. (10) corresponds to the expression of the stomatal blocking fraction for a wet canopy (Brook et al., 1999).  
 252 For dry canopy,  $W_{st}$  always equals 0.  $W_{st}$  is given a value other than 0 only when solar radiation is relatively strong ( $> 200$   
 253  $W.m^{-2}$ ) and the canopy is wet. If rain or dew occurs, the canopy is treated as wet (Zhang et al., 2003b). In this study, as the  
 254 experiments were carried out outside of dew and rain periods, the value of 0 was assigned to  $W_{st}$ .

$$W_{st} = \begin{cases} 0 & SR < 200 \text{ (} W.m^{-2} \text{)} \\ \frac{SR - 200}{800} & 200 < SR < 600 \text{ (} W.m^{-2} \text{)} \\ 0.5 & SR > 600 \text{ (} W.m^{-2} \text{)} \end{cases} \quad (10)$$

255 Mesophyll resistance ( $R_m$ ) is resistance to the diffusion of gas in the mesophyll, preventing it from reaching the  
 256 chloroplasts (Davi, 2004).  $R_m$  depends specifically on the chemical species. For chemical species with very high solubility  
 257 and/or high oxidative power,  $R_m$  is negligible, whereas for chemical species with very low solubility and/or low oxidative  
 258 power,  $R_m$  is assigned a value of  $100 s.m^{-1}$ . For all other chemical species,  $R_m$  is 0 (Zhang et al., 2002b). In view of both the  
 259 very low solubility of iodine ( $I_2$ ) in water (Gottardi, 2001) and its high oxidative power (Carpenter, 2003), a value of 0 has  
 260 been assigned to  $R_m$ .

261 The expression for non-stomatal resistance (Eq. (11)) was the expression determined when parameterising  $R_{ns}$  for  $O_3$   
 262 (Zhang et al., 2002a).

$$\frac{1}{R_{ns}} = \frac{1}{R_{ac} + R_g} + \frac{1}{R_{cut}} \quad (11)$$

263 Where  $R_{ns}$  is the non-stomatal resistance ( $s.m^{-1}$ );  $R_{ac}$  ( $s.m^{-1}$ ) is the canopy aerodynamic resistance;  $R_g$  ( $s.m^{-1}$ ) is the ground  
 264 resistance and  $R_{cut}$  ( $s.m^{-1}$ ) is the cuticle resistance.  $R_{ac}$  does not depend on the chemical species whereas  $R_g$  and  $R_{cut}$  do  
 265 depend on it.

266  $R_{ac}$  is affected by the change in canopy structure including LAI and wind friction velocity.  $R_{ac}$  expression (Eq. (12)) is given  
 267 by Zhang et al. (2002b).

$$R_{ac} = \frac{R_{ac0} \times LAI^{1/4}}{u_*^2} \quad (12)$$

268 Where  $R_{ac0}$  ( $s.m^{-1}$ ) is the reference value for  $R_{ac}$  ( $s.m^{-1}$ ); LAI is leaf area index and  $u^*$  is the wind friction velocity ( $ms^{-1}$ ).  
 269  $R_{ac0}$  values are determined and assigned at many type of canopy including grass. The value of  $R_{ac0}$  ( $50 s.m^{-1}$ ) used in the  
 270 model corresponds to that defined by Wesely (1989) for grassland.  
 271  $R_g$  and  $R_{cut}$  were calculated for  $SO_2$  and  $O_3$ . For all other gases, a formulation to determine  $R_g$  and  $R_{cut}$  (Eq. (13)) was  
 272 developed by Zhang et al, (2003).

$$\frac{1}{R_x(i)} = \frac{\alpha(i)}{R_x(SO_2)} + \frac{\beta(i)}{R_x(O_3)} \quad (13)$$

273 Where  $R_x$  is the ground resistance ( $R_g$ ) or cuticular resistance ( $R_{cut}$ );  $i$  represent the chemical species;  $\alpha$  and  $\beta$  are 2 factors  
 274 based on solubility and semi-redox reactivity of  $i$  (Wesely, 1989).  
 275 Previous studies have suggested that  $R_c$  of iodine would be identical to that of  $SO_2$  (Brandt et al., 2002). As the parameters  $\alpha$   
 276 and  $\beta$  for iodine are not known, approximations have been made. Iodine like  $SO_2$  has high semi-redox reactivity. Although  
 277 the solubility in water at  $25^\circ C$  of iodine ( $0.34 g.L^{-1}$ ) (Hartley and Campbell, 1908) is much lower than that of  $SO_2$  ( $82.4 g.L^{-1}$ )  
 278 (Byerley et al., 1980), as long as the quantity of iodine emitted in atmosphere can be dissolved and oxidized on the grass  
 279 surface, solubility and semi-redox reactivity may be considered as not a limiting factors and, consequently that parameters  
 280  $R_g$  and  $R_{cut}$  of  $SO_2$  can be used for  $I_2$ .  
 281  $R_g$  is considered depending of surface type. For different chemical species including  $I_2$ ,  $R_g$  would be different depending  
 282 that canopy is dry or wet (dew or rain).  
 283 For a dry canopy,

$$R_{cut} = \frac{R_{cutd0}}{e^{0.03 \times RH} \times LAI^{1/4} \times u_*} \quad (14)$$

284 For a wet canopy,

$$R_{cut} = \frac{R_{cutw0}}{LAI^{1/2} \times u_*} \quad (15)$$

285 Where  $R_{cutd0}$  ( $s.m^{-1}$ ) and  $R_{cutw0}$  ( $s.m^{-1}$ ) represent the reference values of  $R_{cut}$  ( $s.m^{-1}$ ) for dry and wet canopy, respectively; RH  
 286 is relative humidity (%); LAI is the leaf area index and  $u^*$  is the wind friction velocity ( $ms^{-1}$ ).  
 287 The reference values  $R_{g0}$  ( $100 ms^{-1}$ ) used in this study is that for  $SO_2$  for grass (Zhang et al., 2003a). As the experiments  
 288 were carried out outside of dew and rain periods, the reference value  $R_{cutd0}$  ( $1000 s.m^{-1}$ ) used is that for  $SO_2$  for grass in dry  
 289 conditions (Zhang et al., 2003a).  
 290 Equations. (16) and (17) are the resultants of the integration of the expressions for  $R_{ac}$ ,  $R_g$  and  $R_{cut}$  in Eq. (11). The  
 291 expression for  $R_{ns}$  becomes:  
 292 For a dry canopy,

$$\frac{1}{R_{ns}} = \frac{1}{R_{ac0} u^{*-2} LAI^{0.25} + R_{g0}} + \frac{1}{R_{cut0} e^{(-0.03 RH)} LAI^{-0.25} u^{*-1}} \quad (16)$$

293 For a wet canopy,

$$\frac{1}{R_{ns}} = \frac{1}{R_{ac0} u^{*-2} LAI^{0.25} + R_{g0}} + \frac{1}{R_{cut0} LAI^{-0.5} u^{*-1}} \quad (17)$$

294 A LAI of 1.50 was used as an input parameter to calculate the non-stomatal resistance. This value was set as a result of the  
 295 measurements made with the LAI-meter. The meteorological parameters used to model the non-stomatal resistance are  
 296 given in Table 7 and Table 8.

### 297 3. Results and discussion

#### 298 *A. Measurement of iodine dry deposition velocities on grass*

299 The iodine concentrations measured in blanks flasks and filters were below the detection limit (see Appendix 1 and  
 300 2). Consequently, there was no transformation of iodine during emission and iodine measured in samples corresponds to  
 301 that emitted using iodine generator.

302 To determine the quantity of iodine in grass tests, the quantity of iodine in blank grass is subtracted from the quantity  
 303 of iodine measured in grass tests. Extraction efficiency is determined by dividing the quantity of iodine measured in grass  
 304 tests to the quantity of iodine added. This ratio is expressed as a percentage. For the 12 tests performed, the mean extract ion  
 305 efficiency was 57% with a ratio of standard deviation to mean (RSD) of 6.44%. These results validated the technique for  
 306 separation of the iodine as I<sub>2</sub> form deposited on the grass. The quantity of iodine measured on the grass blank was 0.14 ±  
 307 0.01 µg.g<sup>-1</sup> of fresh grass (mass ± RSD for the extraction efficiency applied to the mass). The application of this technique  
 308 to the samples resulting from the iodine emissions determined the iodine dry deposition velocities.

310 **Table 5:** Dry deposition velocities of gaseous elemental iodine (<sup>127</sup>I) on grass during MIOSEC 2.

Date and time	Atmospheric iodine concentration in µg.m <sup>-3</sup>	Dry deposition flux of iodine in µg.m <sup>-2</sup> .s <sup>-1</sup>	Dry deposition velocity of iodine in cm.s <sup>-1</sup>
19/09/2018 10:32	110.6	0.078	0.07 ± 0.005
19/09/2018 15:00	29.7	0.076	0.25 ± 0.016
20/09/2018 09:30	18.4	0.010	0.06 ± 0.004
20/09/2018 14:32	48.7	0.063	0.13 ± 0.008
20/09/2018 17:30	30.9	0.039	0.13 ± 0.008
21/09/2018 15:00	46.5	0.046	0.10 ± 0.006
21/09/2018 18:30	116.7	0.024	0.02 ± 0.001
22/09/2018 09:30	117.6	0.081	0.07 ± 0.005
22/09/2018 17:00	15.2	0.042	0.28 ± 0.018
24/09/2018 10:30	20.9	0.058	0.28 ± 0.018
24/09/2018 16:30	16.1	0.079	0.49 ± 0.032
25/09/2018 09:30	4.7	0.012	0.25 ± 0.016
26/09/2018 10:00	4.9	0.002	0.04 ± 0.003

27/09/2018 10:30	132.9	0.399	0.30 ± 0.019
------------------	-------	-------	--------------

311

312 The dry deposition velocities measured during MIOSEC 2 (Table 5) are between 0.02 and 0.49 cm.s<sup>-1</sup>.

313

314 **Table 6:** Dry deposition velocities of gaseous elemental iodine (<sup>127</sup>I) on grass during MIOSEC 3.

Date and time	Atmospheric iodine concentration in $\mu\text{g.m}^{-3}$	Dry deposition flux of iodine in $\mu\text{g.m}^{-2}.\text{s}^{-1}$	Dry deposition velocity of iodine in $\text{cm.s}^{-1}$
04/06/2019 16:05	11.8	0.15	1.25 ± 0.08
04/06/2019 17:32	8.8	0.08	0.87 ± 0.06
06/06/2019 07:35	44.6	0.21	0.48 ± 0.03
06/06/2019 10:30	13.2	0.10	0.73 ± 0.05
06/06/2019 12:30	18.9	0.13	0.69 ± 0.04
06/06/2019 16:03	12.3	0.08	0.63 ± 0.04
07/06/2019 09:55	28.2	0.32	1.15 ± 0.07
07/06/2019 10:47	15.3	0.17	1.10 ± 0.07

315

316 During MIOSEC 3, the dry deposition velocities measured (Table 6) are between 0.48 and 1.25 cm.s<sup>-1</sup>.317 *B. Environmental (including meteorological) variable measurements*

318 The meteorological data obtained using the ultrasonic anemometer and the weather station during the experiment

319 periods are presented in Table 7 and Table 8, which correspond to MIOSEC 2 and MIOSEC 3 respectively.

320

321 **Table 7:** Meteorological data for the 14 experiments conducted during MIOSEC 2.

Date and time	Ts (°C)	S ( $\text{W.m}^{-2}$ )	H ( $\text{W.m}^{-2}$ )	RH (%)	u* ( $\text{m.s}^{-1}$ )	1/L	Stability
19/09/2018 10:32	21	426	75	71	0.16	-0.268	Unstable
19/09/2018 15:00	26	798	211	39	0.37	-0.059	Unstable
20/09/2018 09:30	18	286	14	97	0.07	-0.584	Unstable
20/09/2018 14:32	27	782	181	36	0.26	-0.145	Unstable
20/09/2018 17:30	28	386	84	36	0.24	-0.089	Unstable
21/09/2018 15:00	20	653	169	47	0.33	-0.069	Unstable
21/09/2018 18:30	17	115	9	47	0.22	-0.012	Neutral
22/09/2018 09:30	12	119	9	95	0.05	-0.826	Unstable
22/09/2018 17:00	22	475	83	31	0.35	-0.029	Unstable
24/09/2018 10:30	12	433	71	71	0.36	-0.022	Unstable
24/09/2018 16:30	18	542	165	37	0.53	-0.016	Neutral
25/09/2018 09:30	10	272	27	66	0.36	-0.008	Neutral
26/09/2018 10:00	12	340	38	57	0.15	-0.169	Unstable
27/09/2018 10:30	19	435	45	45	0.26	-0.038	Unstable

322

323 **Table 8:** Meteorological data for the 8 experiments conducted during MIOSEC 3.

Date and time	Ts (°C)	S ( $\text{W.m}^{-2}$ )	H ( $\text{W.m}^{-2}$ )	RH (%)	u* ( $\text{m.s}^{-1}$ )	1/L	Stability
04/06/2019 16:05	20	216	47	63	0.47	-0.005	Neutral
04/06/2019 17:32	19	293	39	69	0.31	-0.018	Neutral
06/06/2019 07:35	9	58	6	100	0.12	0.027	Stable
06/06/2019 10:30	13	344	59	84	0.23	-0.068	Unstable
06/06/2019 12:30	16	644	89	60	0.24	-0.090	Unstable
06/06/2019 16:03	19	725	94	46	0.33	-0.038	Unstable

07/06/2019 09:55	12	180	17	95	0.43	-0.001	Neutral
07/06/2019 10:47	14	389	83	86	0.47	-0.011	Neutral

324

325 *C. Modelling of the dry deposition velocities of iodine*

326 The iodine dry deposition velocities obtained by the model are between 0.11  $\text{cm.s}^{-1}$  and 0.51  $\text{cm.s}^{-1}$  during  
327 MIOSEC 2 (Table 9) and between 0.31  $\text{cm.s}^{-1}$  and 1.60  $\text{cm.s}^{-1}$  during MIOSEC 3 (Table 10).

328

329 **Table 9:** Dry deposition velocities of iodine produced by the model during MIOSEC 2.

Date and time	$R_a$ ( $\text{s.m}^{-1}$ )	$R_b$ ( $\text{s.m}^{-1}$ )	$R_{st}$ ( $\text{s.m}^{-1}$ )	$R_c$ ( $\text{s.m}^{-1}$ )	$V_d$ ( $\text{cm.s}^{-1}$ )
19/09/2018 10:32	11	2	12219	505	0.19
19/09/2018 15:00	6	1	11734	294	0.33
20/09/2018 09:30	19	6	14988	641	0.15
20/09/2018 14:32	8	1	11953	492	0.20
20/09/2018 17:30	9	2	14923	562	0.17
21/09/2018 15:00	7	1	10937	316	0.31
21/09/2018 18:30	16	2	40963	533	0.18
22/09/2018 09:30	20	7	45588	903	0.11
22/09/2018 17:00	6	1	11844	356	0.28
24/09/2018 10:30	6	1	14803	188	0.51
24/09/2018 16:30	7	1	11519	193	0.50
25/09/2018 09:30	10	1	20977	206	0.46
26/09/2018 10:00	13	3	15917	749	0.13
27/09/2018 10:30	9	1	12169	453	0.22

330

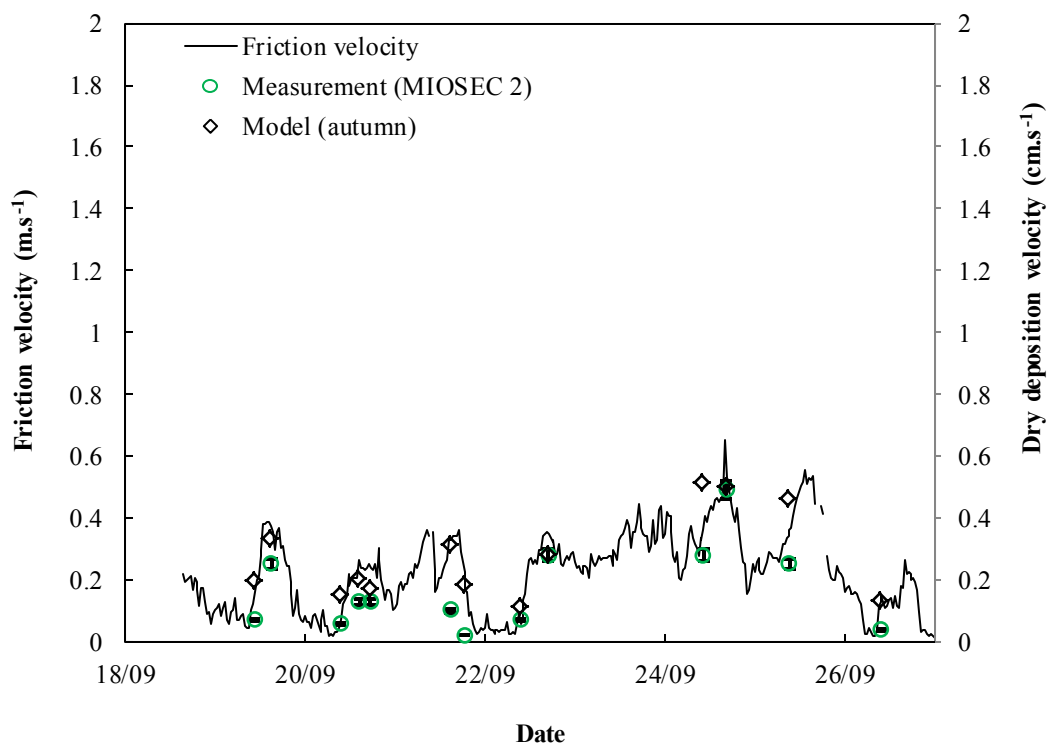
331 **Table 10:** Dry deposition velocities of iodine produced by the model during MIOSEC 3.

Date and time	$R_a$ ( $\text{s.m}^{-1}$ )	$R_b$ ( $\text{s.m}^{-1}$ )	$R_{st}$ ( $\text{s.m}^{-1}$ )	$R_c$ ( $\text{s.m}^{-1}$ )	$V_d$ ( $\text{cm.s}^{-1}$ )
04/06/2019 16:05	8	2	111	66	1.32
04/06/2019 17:32	11	3	88	71	1.17
06/06/2019 07:35	51	7	1108	263	0.31
06/06/2019 10:30	10	4	90	76	1.12
06/06/2019 12:30	9	5	68	101	0.87
06/06/2019 16:03	7	4	65	93	0.96
07/06/2019 09:55	8	2	159	59	1.45
07/06/2019 10:47	8	2	84	53	1.60

332

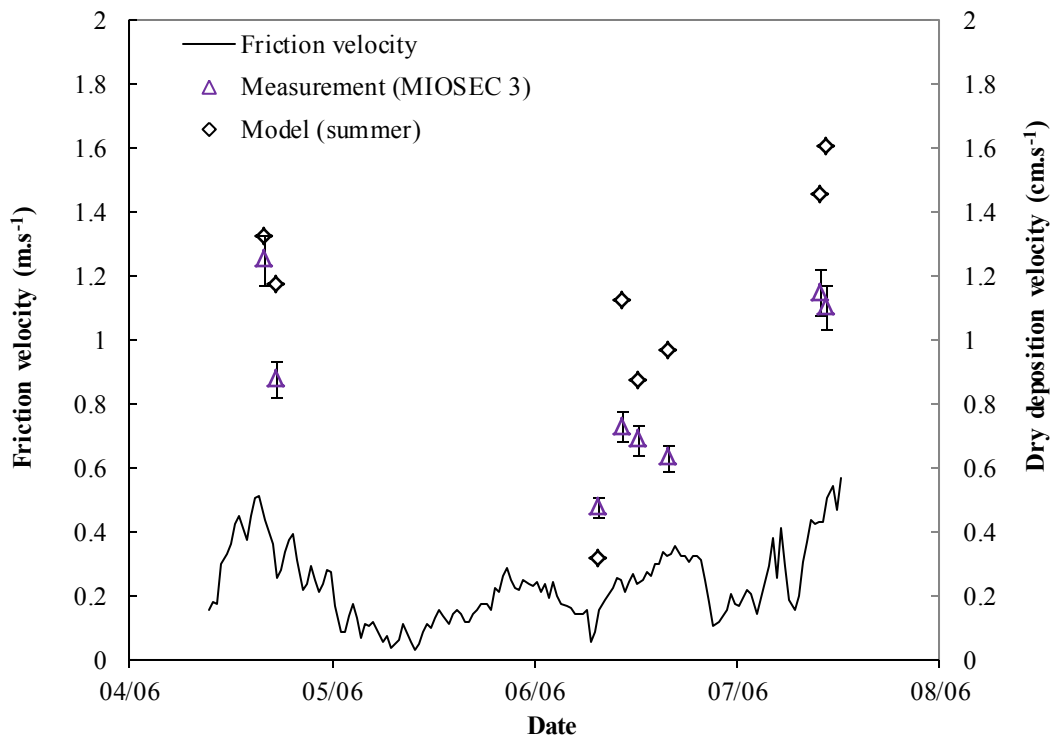
333 *D. Change in the dry deposition velocities of iodine as a function of environmental variables and the*  
334 *physiological properties of the grass*

335 During MIOSEC 2, the deposition velocities varied by more than an order of magnitude and values produced by the  
336 model varied as the same of measurements results. Although the data is very limited on statistical significance, the reasons to  
337 affect the dry deposition velocity during MIOSEC 2 are the mechanical turbulence and, more specifically, in the wind  
338 friction velocity (Fig. 3). These differences are due to the variations existing between the wind friction velocities  
339 (approximately on order of magnitude) measured at the same moment of experiments. Deposition velocities are higher  
340 during the periods of strong winds than during periods of light winds. This observation is corroborated by the significance  
341 level of the correlation (Fig. 5) of the modelled deposition velocities ( $V_{d_{mod}}$ ) with the wind friction velocities ( $u^*$ ) ( $V_{d_{mod}} =$   
342  $1.0 \times u^*$ ,  $R^2 = 0.7$ ). In other words, the iodine deposition on the grass due to entrainment of iodine onto the surface of the  
343 blades of grass by the wind friction velocity is related to surface area. Unlike wind friction velocity, the correlation of  
344 deposition velocities with sensible heat flux and stomatal resistance is not significant. Furthermore, in view of the stomatal  
345 resistances ( $R_{st}$ ) determined during MIOSEC 2, the model shows that the experiments were conducted during a period of the  
346 year (autumn) when the stomata were only slightly open. Consequently, the deposition velocities were dependent on the  
347 non-stomatal resistance ( $R_{ns}$ ), which is also dependent on the wind friction velocity.

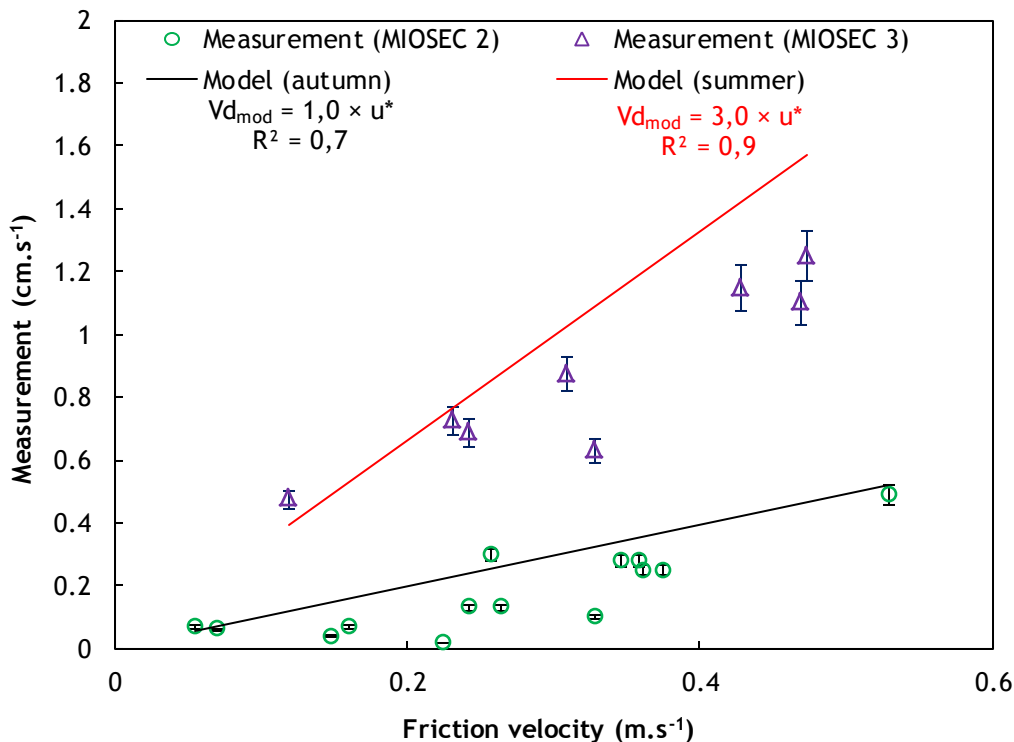


348  
349 Fig. 3. Change in dry deposition velocities of gaseous elemental iodine and wind friction velocities during  
350 MIOSEC 2: the bar on the deposition velocities (circles) corresponds to the mean standard deviation divided by the mean as  
351 a percentage for the extraction efficiency (RSD = 6.34%).  
352

353 During MIOSEC 3, the variations in measurements deposition velocities are the same to values given by model. The first  
 354 reason of variations in deposition velocities is due to the mechanical turbulence. Deposition velocities are higher during  
 355 periods of strong winds than during periods of light winds. The second reason is due to the stomata opening. For the same  
 356 values of friction velocities, dry deposition velocities obtained during MIOSEC 3 are 2 to 3 times higher than those obtained  
 357 during MIOSEC 2. The model shows that the stomatal resistances were smaller during MIOSEC 3 than those obtained  
 358 during MIOSEC 2. In other words, the experiments were conducted during a period of the year (summer) when the stomata  
 359 were more open. Consequently, the dry deposition velocities were higher in this period. The change in deposition velocity  
 360 during MIOSEC 3 shows that the dry deposition of iodine was favoured not only by the wind friction velocity (Fig. 4) but  
 361 also by iodine penetration into the blades of grass due to the openness of the stomata. This is reflected in the high  
 362 significance level of the correlation (Fig. 5) of the modelled deposition velocities with the wind friction velocities ( $Vd_{\text{mod}} =$   
 363  $3.0 \times u^*$ ,  $R^2 = 0.9$ ).



364  
 365 Fig. 4. Change in dry deposition velocities of gaseous elemental iodine and wind friction velocities during MIOSEC 3: the  
 366 bar on the deposition velocities (triangles) corresponds to the mean standard deviation divided by the mean as a percentage  
 367 for the extraction efficiency (RSD = 6.34%).



368

369

Fig. 5. Change in dry deposition velocities of gaseous elemental iodine during MIOSEC 2 (circles) and MIOSEC 3 (triangles) as a function of the wind friction velocities: the bar on the deposition velocities corresponds to the mean standard deviation divided by the mean as a percentage for the extraction efficiency (RSD = 6.34%).

370

371

372

373

### E. Comparison of the measured dry deposition velocities with the modelled dry deposition velocities

374

The measured dry deposition velocities are comparable with the modelled dry deposition velocities and, when the former are related by a function to the latter for each of the measurement campaigns, they correlate linearly with correlation coefficients ( $R^2$ ) of 0.61 and 0.71 for MIOSEC 2 (Fig. 6) and MIOSEC 3 (Fig. 7), respectively. The measured data are generally 15-30% lower than those modelling results during both MIOSEC 2 and 3. The average of the deviations in absolute value compared to the measured values (Mean Absolute Percentage Error, MAPE) is 10% and 5% during MIOSEC 2 and 3, respectively. Knowing that the solubility of  $\text{SO}_2$  is higher than that  $\text{I}_2$  and  $R_{g0}$  and  $R_{cut0}$  being parameters based on solubility and semi-redox reactivity of the gaseous specie, the overestimated results of model could be explained by the fact that approximations consisting to apply values references of  $R_{g0}$  and  $R_{cut0}$  from  $\text{SO}_2$  to  $\text{I}_2$  were used in the model in place of the reference values specific to  $\text{I}_2$ . The model can be improved as a determining the parameters  $R_{g0}$  and  $R_{cut0}$  specific to  $\text{I}_2$ .

383

To conclude, the modelled dry deposition velocities and the measured dry deposition velocities show that the dry deposition of iodine is dependent on surface resistance ( $R_c$ ), which is depends on stomatal resistance ( $R_{st}$ ) and non-stomatal resistance ( $R_{ns}$ ). The model also shows that stomatal resistance is lower in summer than in autumn, whereas non-stomatal resistance varies very slightly through the seasons and is dependent on the wind friction velocity ( $u^*$ ). Consequently, when stomatal resistance is high, which coincides with closure of the stomata, dry deposition velocities are lower and are

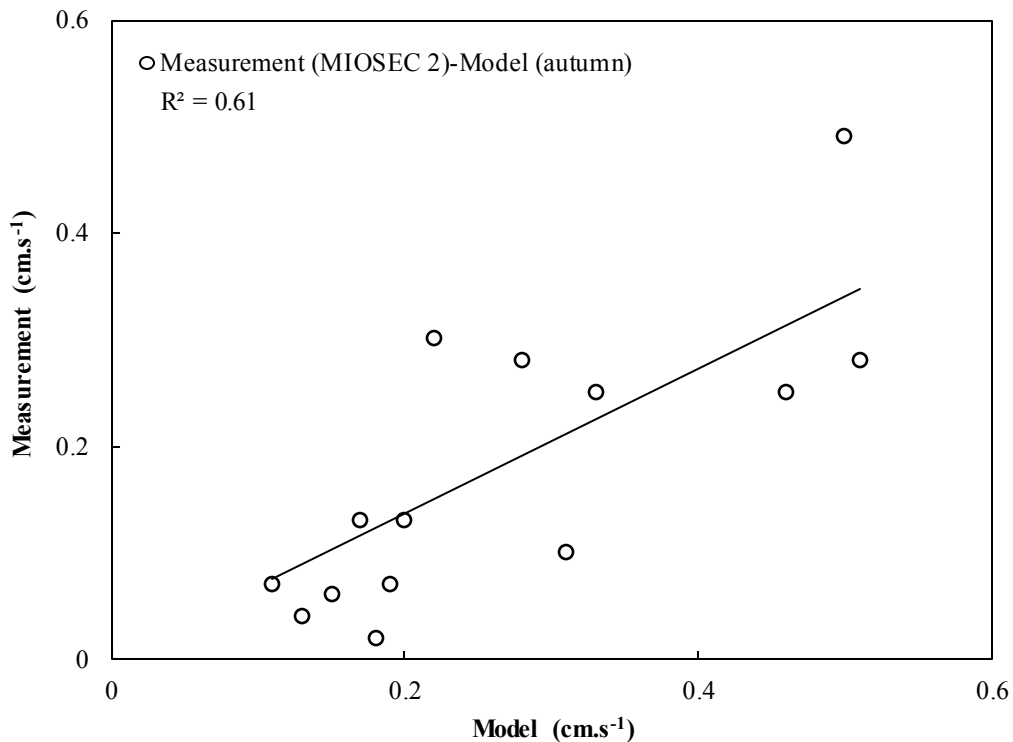
384

385

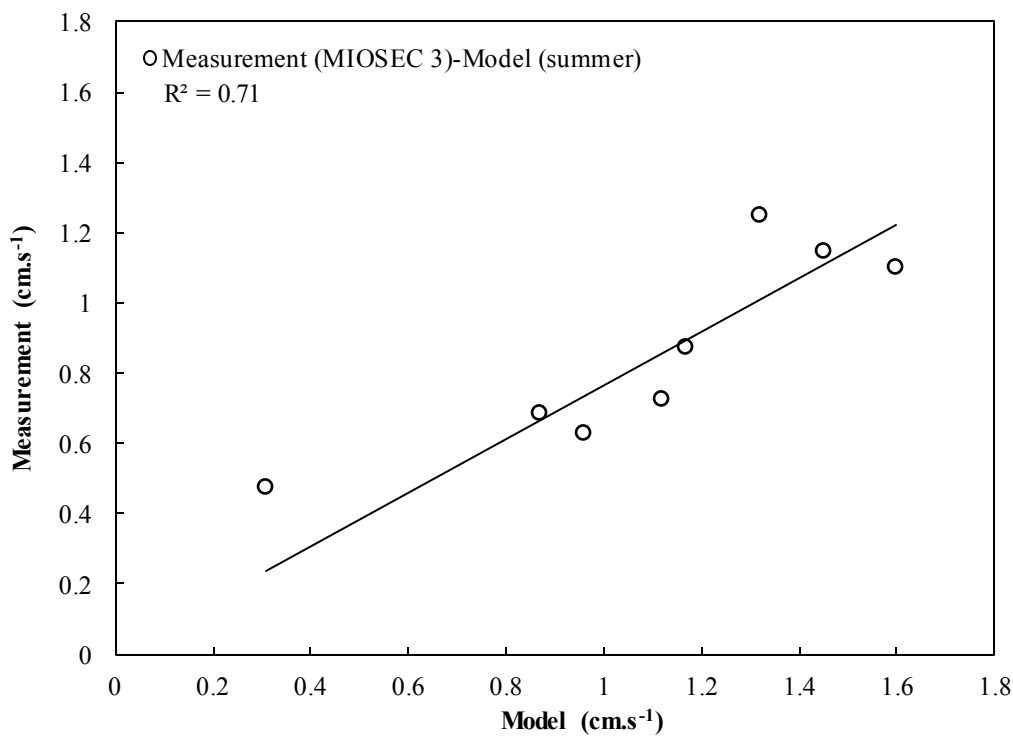
386

387

388 dependent on the wind friction velocities. When stomatal resistance falls, which coincides with opening of the stomata, the  
389 deposition velocities increase and depend on both the wind friction velocities and the openness of the stomata.



390  
391 **Fig. 6.** Comparison of measured dry deposition velocities with modelled dry deposition velocities during MIOSEC 2.



392  
393 **Fig. 7.** Comparison of measured dry deposition velocities with modelled dry deposition velocities during MIOSEC 3.

394 *F. Comparison with the data in the literature*

395 Numerous data related to determination of the dry deposition velocities of iodine exist in the literature (Table 11).  
396 These values are by no means exhaustive but only examples. The deposition velocities of I<sub>2</sub> has been measured to a range of  
397 different surfaces both in the outdoor and indoor environment including skin and relate to both stable iodine (<sup>127</sup>I) and  
398 radioactive iodine (<sup>129</sup>I, <sup>131</sup>I) in their elemental or particulate forms.

399 It is mentioned in table 11 that certain dry deposition velocities of iodine corresponded to those iodine in particulate  
400 form, it should be remember here the reasons of the differences in these deposition with those of elementary iodine  
401 measured in this study. These differences are due to the fact that the diffusivity of gases is greater than that of particles.

402 For experiments conducted in the environment, the data reported showed that dry deposition velocities for iodine  
403 were between 0.001 and 1 cm.s<sup>-1</sup> (Handge and Hoffman, 1974), which means that the data were spread across three orders  
404 of magnitude. The dry deposition velocities measured in that study are similar to those reported here, though the data  
405 dispersion is significantly smaller for the data acquired during MIOSEC 3 (0.48-1.25 cm.s<sup>-1</sup>) and is limited to one order of  
406 magnitude in MIOSEC 2 (0.02-0.49 cm.s<sup>-1</sup>). Concerning the dry deposition velocities of gaseous elemental iodine, the  
407 measurements presented by many studies are spread across several orders of magnitude. For example, measurements taken  
408 on grass by Chamberlain and Chadwick (1966) led to the conclusion that the dry deposition velocity of elemental iodine  
409 (<sup>131</sup>I) was 1.8 cm.s<sup>-1</sup>. Most authors suggest taking 1 cm.s<sup>-1</sup> as the dry deposition velocity of elemental iodine, though  
410 Heinemann and Vogt (1980) suggest 2 cm.s<sup>-1</sup>. The mean of the deposition velocities measured in this study during  
411 MIOSEC 3 (0.86 cm.s<sup>-1</sup>) is similar to the value suggested in the other studies (1 cm.s<sup>-1</sup>). For MIOSEC 2, two main reasons  
412 could explain the difference between these suggested values and the values obtained.

413 The first reason could be the time of day when the dry deposition velocities were measured and the variations in the  
414 meteorological parameters, including wind friction velocity, temperature and solar radiation. During this study, the dry  
415 deposition velocities measured during MIOSEC 2 did indeed vary in the course of the experiments, in line with the  
416 variations in wind friction velocity.

417 The second possible reason could be the period of the year when the measurements were taken. Measurements of <sup>127</sup>I  
418 have led to the calculation of dry deposition velocities of 0.16 cm.s<sup>-1</sup> (Chamberlain and Chadwick, 1966), similar to the  
419 mean of the dry deposition velocities obtained in this study during MIOSEC 2 (0.18 cm.s<sup>-1</sup>). The results obtained in this  
420 study during MIOSEC 2 are also similar to those obtained when determining the dry deposition velocities for O<sub>3</sub> on  
421 grassland at night, i.e. when the stomata were closed, so when the dry deposition velocities were strictly linked to surface  
422 resistance, which is inversely linked to wind friction velocity (Zhang et al., 2002b). According to the model produced  
423 during this study, the dry deposition velocities of iodine depend on the surface resistance (R<sub>c</sub>), which is a combination of  
424 non-stomatal resistance (R<sub>ns</sub>) and stomatal resistance (R<sub>st</sub>). The model showed that R<sub>ns</sub> varies only very slightly through the  
425 seasons of the year and depends on the wind friction velocity (u\*). The model also showed that R<sub>st</sub> is higher in autumn,  
426 when the stomata are closed, than in summer, when the stomata are open. For example, the deposition velocities measured  
427 in this study were higher in summer (MIOSEC 3) than in autumn (MIOSEC 2). The mean surface resistance given by the  
428 model was 456 s.m<sup>-1</sup> for MIOSEC 2 and 98 s.m<sup>-1</sup> for MIOSEC 3. If reference were made to Chamberlain and Chadwick  
429 (1966), who suggested taking R<sub>c</sub> = 500 s.m<sup>-1</sup> when determining the dry deposition velocities of gaseous <sup>131</sup>I, then the dry  
430 deposition velocities of iodine would be deemed not to change throughout the seasons, which contradicts our observations.

431 **Table 11:** Dry deposition velocities of iodine reported in the literature.

Dry deposition velocity (cm.s <sup>-1</sup> )	Test specimens	Observations	Reference
10 <sup>-3</sup> -1	Grass	Review, <sup>131</sup> I.	(Handge and Hoffman, 1974)
0.1-1.5	Grass	Elemental and particulate iodine, <sup>131</sup> I.	(Eggleton et al., 1963)
0.1-0.5	Grass	Fallout from Fukushima measured in France, <sup>131</sup> I.	(Parache et al., 2011)
0.54	Grass	Calculation of iodine deposits from data reported for distant nuclear explosions in the British Isles.	(Chamberlain and Chadwick, 1966)
0.5	Grass	Calculation of iodine deposits from data reported for distant nuclear explosions, Brookhaven, Long Island.	(Hull, 1963)
0.58	Grass	Air stack at the Karlsruhe reprocessing plant, <sup>129</sup> I.	(Wershofen and Aumann, 1989)
0.5	Grass	Elemental and particulate iodine, <sup>131</sup> I.	(Hull, 1963)
0.3	Grass	Elemental and particulate iodine, <sup>131</sup> I.	(Clark and Smith, 1988)
0.8	Grass	Elemental iodine, <sup>131</sup> I.	(Chamberlain, 1959)
1.8	Grass	Field experiments, elemental iodine.	(Chamberlain and Chadwick, 1966)
2	Grass	Elemental iodine, <sup>131</sup> I.	(Heinemann and Vogt, 1980)
(0.5 – 3.3) × 10 <sup>-3</sup>	Grass	Environmental chamber, <sup>127</sup> I.	(Karunakara et al., 2018)
5.4 × 10 <sup>-5</sup>	Bean leaf	Environmental chamber, <sup>131</sup> I.	(Singhal et al., 2004)

432

433

434

435

436

437

438

Finally, based on closed field experiments (environmental chamber), with the emission of gaseous <sup>127</sup>I on grass, Karunakara et al. (2018) propose dry deposition velocities of (0.51-3.3) × 10<sup>-3</sup> cm.s<sup>-1</sup>, whereas with the emission of gaseous <sup>131</sup>I on bean leaves, Singhal et al. (2004) propose 5.4 × 10<sup>-5</sup> cm.s<sup>-1</sup>. These values differ by several orders of magnitude from those obtained during this study and from data produced during experiments in the environment. These differences are due to the fact that, in an open atmosphere, deposition is controlled by atmospheric turbulence.

439

#### 4. Conclusion

440

441

442

443

444

445

446

447

448

449

450

451

452

An experimental methodology based on emissions of gaseous elemental iodine (I<sub>2</sub>) into the atmosphere in the middle of grassland was developed to determine the dry deposition velocities of iodine. The dry deposition velocities measured during MIOSEC 2 are between 0.02 and 0.50 cm.s<sup>-1</sup>, a range covering one order of magnitude. The dry deposition velocities measured during the MIOSEC 3 campaign are between 0.48 and 1.25 cm.s<sup>-1</sup>. As a result of these experiments, a model for the dry deposition of iodine was developed. This model is based on the gas dry deposition principle. The input parameters for the model were the micrometeorological characteristics of the atmospheric surface layer, the physico-chemical properties of the iodine and the surface properties of the grass, all measured at the time of the experiments. The deposition velocities produced by the model are between 0.11 and 0.51 cm.s<sup>-1</sup> for the MIOSEC 2 campaign and between 0.31 and 1.60 cm.s<sup>-1</sup> for the MIOSEC 3 campaign. For both campaigns, the measured dry deposition velocities are comparable with the modelled dry deposition velocities and when the former are related by a function to the latter, they correlate linearly with significant correlation coefficients. Consequently, this study qualifies the model's input parameters. The model showed that the variations between deposition velocities are due to variations in the wind friction velocities measured at the time of the experiments. The model also showed that the deposition velocities changed through the different seasons of the year. The

453 deposition velocities are higher in summer, when the openness of the stomata is at its maximum. The deposition velocities  
 454 measured in summer (MIOSEC 3) depend on both the wind friction velocities and the openness of the stomata. They are  
 455 lower in autumn when they are mainly dependent on the wind friction velocities because of the closure of the stomata. The  
 456 data obtained during this study agree with those reported in the literature for experiments conducted under the same  
 457 conditions. However, they differ from the data obtained during experiments conducted in experimental chambers where  
 458 there is no atmospheric turbulence. It should be noted that this study consisting of modelling the deposition of I<sub>2</sub> and  
 459 comparing the results of model with values obtained experimentally is original. To improve model, the approximations  
 460 made must be replaced by the parameters specific to I<sub>2</sub>. The model is not suitable for atmospheric process for prognostic  
 461 pollution models, as it requires measurement of a range of parameters. However, it remains applicable to iodine deposition  
 462 because it predicts I<sub>2</sub> dry deposition depending on atmospheric turbulence parameters and surfaces properties of plant cover  
 463 and may be used to learn about parametric influences. The model developed in this study will be tested on releases of  
 464 gaseous radioactive iodine (<sup>129</sup>I) and under different conditions, particularly a longer release time (2 weeks) and a greater  
 465 distance between the release point and the sampling site (2 km).

## 466 Acknowledgements

467 We would like to thank the entire INRA team for giving us permission to conduct the experimental campaigns  
 468 (MIOSEC) on their site and for making their laboratory available to us to carry out the measurements.

469  
 470 **Appendix 1:** Atmospheric iodine concentrations on filters, in blank NaOH and in NaOH samples during MIOSEC 2.  
 471

Date and time	Atmospheric iodine concentration (µg.L <sup>-1</sup> ) on filters in NaOH 0.5 N	Atmospheric iodine concentration (µg.L <sup>-1</sup> ) in blank NaOH 0.5 N	Atmospheric iodine concentration (µg.L <sup>-1</sup> ) in samples in NaOH 0.5 N	Volume (L) of NaOH 0.5 N in flask for atmospheric iodine samples	Atmospheric iodine concentration (µg)	Volume (L) of air sampled	Atmospheric iodine concentration (µg.m <sup>-3</sup> )
19/09/2018 10:32	< 2.5	< 2.5	66.3	0.1	6.6	60	110.6
19/09/2018 15:00	< 2.5	< 2.5	17.8	0.1	1.8	60	29.7
20/09/2018 09:30	< 2.5	< 2.5	11.0	0.1	1.1	60	18.4
20/09/2018 14:32	< 2.5	< 2.5	29.2	0.1	2.9	60	48.7
20/09/2018 17:30	< 2.5	< 2.5	18.5	0.1	1.9	60	30.9
21/09/2018 15:00	< 2.5	< 2.5	27.9	0.1	2.8	60	46.5
21/09/2018 18:30	< 2.5	< 2.5	70.0	0.1	7.0	60	116.7
22/09/2018 09:30	< 2.5	< 2.5	70.5	0.1	7.1	60	117.6
22/09/2018 17:00	< 2.5	< 2.5	9.1	0.1	0.9	60	15.2

24/09/2018 10:30	< 2.5	< 2.5	12.5	0.1	1.3	60	20.9
24/09/2018 16:30	< 2.5	< 2.5	9.6	0.1	1.0	60	16.1
25/09/2018 09:30	< 2.5	< 2.5	2.8	0.1	0.3	60	4.7
26/09/2018 10:00	< 2.5	< 2.5	3.0	0.1	0.3	60	4.9
27/09/2018 10:30	< 2.5	< 2.5	79.7	0.1	8.0	60	132.9

472

473

474

475

**Appendix 2:** Atmospheric iodine concentrations on filters, in blank NaOH and in NaOH samples during MIOSEC 3.

Date and time	Atmospheric iodine concentration ( $\mu\text{g.L}^{-1}$ ) on filters in NaOH 0.5 N	Atmospheric iodine concentration ( $\mu\text{g.L}^{-1}$ ) in blank NaOH 0.5 N	Atmospheric iodine concentration ( $\mu\text{g.L}^{-1}$ ) in samples in NaOH 0.5 N	Volume (L) of NaOH 0.5 N in flask for atmospheric iodine samples	Atmospheric iodine concentration ( $\mu\text{g}$ )	Volume (L) of air sampled	Atmospheric iodine concentration ( $\mu\text{g.m}^{-3}$ )
04/06/2019 16:05	< 2.5	< 2.5	7,1	0,1	0,7	60	11,8
04/06/2019 17:32	< 2.5	< 2.5	5,3	0,1	0,5	60	8,8
06/06/2019 07:35	< 2.5	< 2.5	26,7	0,1	2,7	60	44,6
06/06/2019 10:30	< 2.5	< 2.5	7,9	0,1	0,8	60	13,2
06/06/2019 12:30	< 2.5	< 2.5	11,3	0,1	1,1	60	18,9
06/06/2019 16:03	< 2.5	< 2.5	7,4	0,1	0,7	60	12,3
07/06/2019 09:55	< 2.5	< 2.5	16,9	0,1	1,7	60	28,2
07/06/2019 10:47	< 2.5	< 2.5	9,2	0,1	0,9	60	15,3

476

477

478

479

## References

480

Arya, S.P., 1999. Air pollution meteorology and dispersion. Oxford University Press New York.

481

Brandt, J., Christensen, J.H., Frohn, L.M., 2002. Modelling transport and deposition of caesium and iodine from the Chernobyl accident using the DREAM model. Atmos. Chem. Phys. 2, 397-417.

482

Brook, J.R., Zhang, L., Di-Giovanni, F., Padro, J., 1999. Description and evaluation of a model of deposition velocities for routine estimates of air pollutant dry deposition over North America.: Part I: model development. Atmospheric Environment 33, 5037-5051.

483

Byerley, J.J., Rempel, G.L., Le, V.T., 1980. Solubility of sulfur dioxide in water-acetonitrile solutions. Journal of Chemical and Engineering Data 25, 55-56.

484

Carpenter, L.J., 2003. Iodine in the Marine Boundary Layer. Chemical Reviews 103, 4953-4962.

488 Chamberlain, A.C., Chadwick, R.C., 1966. Transport of iodine from atmosphere to ground. *Tellus* 18, 226-237.

489 Davi, H., 2004. Développement d'un modèle forestier générique simulant les flux et les stocks de carbone et d'eau dans le  
490 cadre des changements climatiques. Université Paris XI, Orsay.

491 Forsythe, W., 1956. *Smithsonian physical tables*: Smithsonian Inst. Washington, DC, Pub 4169.

492 Fuge, R., 1996. Geochemistry of iodine in relation to iodine deficiency diseases. Geological Society, London, Special  
493 Publications 113, 201-211.

494 Gottardi, W., 2001. Iodine and iodine compounds. Disinfection, sterilization, and preservation. Philadelphia: Lippincott  
495 Williams & Wilkins, 159-184.

496 Handge, P., Hoffman, F., 1974. The necessity for environmental surveillance in the evaluation of nuclear power plant sites.

497 Hartley, H., Campbell, N.P., 1908. LXIX.—The solubility of iodine in water. *Journal of the Chemical Society, Transactions*  
498 93, 741-745.

499 Heinemann, K., Vogt, K., 1980. Measurements of the deposition of iodine onto vegetation and of the biological half-life of  
500 iodine on vegetation. *Health Physics* 39, 463-474.

501 Hou, X., Hansen, V., Aldahan, A., Possnert, G., Lind, O.C., Lujaniene, G., 2009. A review on speciation of iodine-129 in  
502 the environmental and biological samples. *Analytica Chimica Acta* 632, 181-196.

503 Karunakara, N., Ujwal, P., Yashodhara, I., Sudeep Kumara, K., Mohan, M.P., Bhaskar Shenoy, K., Geetha, P.V., Dileep,  
504 B.N., James, J.P., Ravi, P.M., 2018. Estimation of air-to-grass mass interception factors for iodine. *Journal of*  
505 *Environmental Radioactivity* 186, 71-77.

506 Nielsen, O.J., 1981. A literature review on radioactivity transfer to plants and soil.

507 Noguchi, H., Murata, M., 1988. Physicochemical speciation of airborne <sup>131</sup>I in Japan from Chernobyl. *Journal of*  
508 *Environmental Radioactivity* 7, 65-74.

509 Padro, J., den Hartog, G., Neumann, H.H., 1991. An investigation of the ADOM dry deposition module using summertime  
510 O<sub>3</sub> measurements above a deciduous forest. *Atmospheric Environment. Part A. General Topics* 25, 1689-1704.

511 Parache, V., Pourcelot, L., Roussel-Debet, S., Orjollet, D., Leblanc, F., Soria, C., Gurriaran, R., Renaud, P., Masson, O.,  
512 2011. Transfer of <sup>131</sup>I from Fukushima to the Vegetation and Milk in France. *Environmental Science & Technology* 45,  
513 9998-10003.

514 Pellerin, G., Maro, D., Damay, P., Gehin, E., Connan, O., Laguionie, P., Hébert, D., Solier, L., Boulaud, D., Lamaud, E.,  
515 Charrier, X., 2017. Aerosol particle dry deposition velocity above natural surfaces: Quantification according to the particles  
516 diameter. *Journal of Aerosol Science* 114, 107-117.

517 Saiz-Lopez, A., Plane, J.M.C., Baker, A.R., Carpenter, L.J., von Glasow, R., Gómez Martín, J.C., McFiggans, G., Saunders,  
518 R.W., 2012. Atmospheric Chemistry of Iodine. *Chemical Reviews* 112, 1773-1804.

519 Sandell, E.B., Kolthoff, I.M., 1937. Micro determination of iodine by a catalytic method. *Microchimica Acta* 1, 9-25.

520 Seinfeld, J.H., 1985. *Atmospheric Chemistry and Physics of Air Pollution* Wiley. New York 986.

521 Seinfeld, J.H., Pandis, S.N., 2016. *Atmospheric chemistry and physics: from air pollution to climate change*. John Wiley &  
522 Sons.

523 Singhal, R., Narayanan, U., Gurg, R., 2004. Estimation of deposition velocities for <sup>85</sup>Sr, <sup>131</sup>I, <sup>137</sup>Cs on spinach, radish  
524 and beans leaves in a tropical region under simulated fallout conditions. *Water, air, and soil pollution* 158, 181-192.

525 Thakur, P., Ballard, S., Nelson, R., 2013. An overview of Fukushima radionuclides measured in the northern hemisphere.  
526 Science of The Total Environment 458-460, 577-613.

527 Truesdale, V.W., Žic, V., Garnier, C., Cukrov, N., 2012. Circumstantial evidence in support of org-I as a component of the  
528 marine aerosol arising from a study of marine foams. Estuarine, Coastal and Shelf Science 115, 388-398.

529 Wesely, M.L., 1989. Parameterization of surface resistances to gaseous dry deposition in regional-scale numerical models.  
530 Atmospheric Environment (1967) 23, 1293-1304.

531 Whitehead, D.C., 1984. The distribution and transformations of iodine in the environment. Environment International 10,  
532 321-339.

533 Wong, G.T.F., 1991. The marine geochemistry of iodine. Rev. Aquat. Sci. 4, 45-73.

534 Zhang, L., Brook, J.R., Vet, R., 2002a. On ozone dry deposition—with emphasis on non-stomatal uptake and wet canopies.  
535 Atmospheric Environment 36, 4787-4799.

536 Zhang, L., Brook, J.R., Vet, R., 2003a. Evaluation of a non-stomatal resistance parameterization for SO<sub>2</sub> dry deposition.  
537 Atmospheric Environment 37, 2941-2947.

538 Zhang, L., Brook, J.R., Vet, R., 2003b. A revised parameterization for gaseous dry deposition in air-quality models. Atmos.  
539 Chem. Phys. 3, 2067-2082.

540 Zhang, L., Moran, M.D., Makar, P.A., Brook, J.R., Gong, S., 2002b. Modelling gaseous dry deposition in AURAMS: a  
541 unified regional air-quality modelling system. Atmospheric Environment 36, 537-560.

542 Zhou, Z., 1995. Evaluation des rejets marins d'iode-129 par les usines de retraitement de la Hague (France) et Sellafield (U.  
543 K.) en vue de leur utilisation comme traceur océanographique. Paris 11.

544